Catalysis Today 443 (2025) 114959

Contents lists available at ScienceDirect

Catalysis Today

journal homepage: www.elsevier.com/locate/cattod

Catalytic behaviour of CuO_x and VO_x on Ti_3SiC_2 support for direct oxidation of methane

Alexandra C. Iacoban [a,b], Toton Haldar [a], Florentina Neaţu [a], Iuliana M. Chirica [a,c], Anca G. Mirea [a], Ştefan Neaţu [a], Michel W. Barsoum [d], Mihaela Florea [a,b,*]

[a] National Institute of Materials Physics, 405A Atomistilor Street, Magurele 077125, Romania
[b] Interdisciplinary School of Doctoral Studies, University of Bucharest, Mihai Kogalniceanu Street 36-46, Bucharest 050067, Romania
[c] University of Bucharest, Faculty of Physics, 405 Atomistilor street, Magurele 077125, Romania
[d] Department of Materials Science & Engineering, Drexel University, Philadelphia, PA 19104, USA

ARTICLE INFO

Keywords:
Direct oxidation of methane (DOM)
Ti_3SiC_2 MAX phase
Formaldehyde
VO_x
CuO_x

ABSTRACT

Herein we show that the Ti_3SiC_2 MAX phase can be used as a support for deposition of different amounts of metal oxides (MO_x, M = Cu or V) (5, 10 and 20 wt%) for the direct oxidation of methane to formaldehyde using molecular oxygen, at relatively low temperatures and atmospheric pressure. The oxides were deposited using a hydrothermal method at 180 °C without affecting the bulk MAX phase structure. However, during the hydrothermal treatment (HT) a thin oxide layer - found to play an important role in the reaction's selectivity– was evidenced by X-ray photoelectron spectroscopy. We thus conclude that the MO_x species are responsible for the CH_4 activation, while the Ti_3SiC_2 surface is responsible for the high selectivity to formaldehyde indicating that, Ti_3SiC_2 has great potential for designing innovative catalysts for direct oxidation of methane using molecular oxygen and at atmospheric pressure.

1. Introduction

Given the growing concerns about the environment and the urgent need to find alternatives for fossil fuels resources for chemicals production is highly necessary. A promising candidate as alternative supply would be methane (CH_4) as it is an abundant natural resource. Additionally, methane is the main component of biogas, a renewable and sustainable source [1,2]. Consequently, a good solution would be to use CH_4 as a source of added value chemicals such as methanol, CH_3OH or formaldehyde, HCHO, which can serve as fundamental component for synthesizing a wide range of beneficial substances and materials. Efforts to accomplish selective direct oxidation of methane, DOM, into CH_3OH and/or HCHO, sometimes referred to as the "dream reaction" [3,4], have been unsuccessful in creating practical industrial processes. Although the process is theoretically feasible [5,6], it presents significant challenges in terms of kinetics [7–9].

This is not an easy task, since CH_4 is quite stable due to its symmetrical tetrahedral structure. Therefore, the major impediment to the DOM reaction is the high energy requirement (440 kJ·mol^{-1}) for activating the C–H bond in the CH_4, as well as the reduced thermodynamic stability of the desired products [9]. These factors typically contribute to the tendency for overoxidation to carbon dioxide, CO_2, and carbon monoxide, CO, which commonly occurs under typical reaction circumstances.

At the beginning of the last century, DOM was first approached by combustion at high pressure [8]. Later, the emergency to develop industrial processes led to studies that provided high selectivity of methanol and formaldehyde (50 %) but only under extreme conditions (400 °C, 50 atm) [10–13]. DOM was further developed using homogenous approaches based on transition-metal, TM, complexes (Pd, Pt, Ir, Rh, Ru or Hg) [14–17], which suffer from limitations such as low turnover frequencies, TOF, utilization of expensive noble metal precursors, difficulty of separation, and reactors' corrosion. These impediments have prevented the approaches for industrial applications.

The majority of catalysts used were derived from transition metal/oxidic compounds, in which the metal served as the active site, while the support was often an inert oxide. This is the "classical" approach of heterogeneous catalysis commonly employed in industrial applications that involve the use of "normal" supported catalysts, where the quantity of metal oxide is significantly larger than the quantity of metal [18–24].

* Corresponding author at: National Institute of Materials Physics, 405A Atomistilor Street, Magurele 077125, Romania.
E-mail addresses: mihaela.florea@infim.ro, mihaela.florea@chimie.unibuc.ro (M. Florea).

https://doi.org/10.1016/j.cattod.2024.114959
Received 11 March 2024; Received in revised form 21 June 2024; Accepted 28 July 2024
Available online 7 August 2024

The limitations of these methods include the significant metal-support interactions that result in a dramatic alteration of the metal's chemisorption characteristics [18–24]. Said otherwise, the oxide layer partially envelops the metal, rendering it incapable of chemisorption and, thus, unable to dissociate hydrocarbons. Schwab et al. were the first to propose the use of an inverted catalyst as a potential solution [24]. This catalyst is created by depositing oxide particles on a metal substrate.

Following the same concept, in this study, we provide a novel idea we are labelling an *"upside down"* catalytic system, where MO_x (M = Cu, V) are supported on a ternary carbide with metallic properties, viz. a Ti_3SiC_2 MAX phase. Our approach diverges from the previously disclosed inverse catalytic system described in reference [24], since our support is not a single crystal. The support we used is the widely recognized MAX phase, layered ternary carbide materials, first discovered in the '60 s [25], but exploited only in the mid-'90 s, by Barsoum and co-workers [26]. The MAX name derives from their composition: $M_{n+1}AX_n$, where M is an early TM, A is an element belonging mostly to group IIIA or IVA, X is C and/or N, and n = 1, 2, or 3 [27,28]. These relatively newly synthesized MAX phases (Ti_3SiC_2, Ti_3AlC, Ti_2AlC, etc.) represent a class of solids with unique properties, bridging the gap between metals and ceramics due to their mostly covalent-metallic bonds. There are more than 300 different MAX phases available nowadays [29]. These layered ternaries possess high thermal and electrical conductivities and are readily machinable. Some have low densities, and good endurance to elevated temperatures [27,30] as well as being oxidation resistant [31], but what renders the MAX phase useful here is their metallic-like electrical conductivity [32]. However, considering all these properties, only a few MAX phases catalytic applications have been reported so far [33,34]. Moreover, because the first identified MAX phase, Ti_3SiC_2 [26], forms, upon oxidation, on its surface a dual oxide with a rutile outer layer, and an inner layer that is a mixture of SiO_2 and rutile [35], we strongly believe that would be a good catalyst capable of chemisorbing and destabilizing the C–H bond.

Regarding the utilization of Cu-based systems for DOM reaction, it is worth noting that the investigation of Cu-based catalysts was very intense. Groothaert *et al.* [36] found that Cu-ZSM-5 (Zeolite Socony Mobil-5) and chemisorbed oxygen, O, was able to catalyze the oxidation of CH_4 to CH_3OH at 125 °C after pretreatment in O_2 at 350 °C, but only a small amount of CH_3OH was produced. Li and coworkers prepared CuO_x/SBA-15 (Santa Barbara Amorphous-15 mesoporous silica) [37] catalyst that demonstrated the highest catalytic efficiency for the production of HCHO in the presence of oxygen (O_2), with a turnover frequency of 5.6 s^{-1}. Aguila *et al.* [38] demonstrated the impact of the supporting materials for CH_4 activation, which exhibits the following order: $CuO/ZrO_2 > CuO/Al_2O_3 \gg CuO/SiO_2$.

Similar advancements have been achieved in the development of V-based catalysts that exhibit high levels of performance in the DOM reaction to CH_3OH and/or HCHO [39,40]. Loricela *et al.* [41] synthesized a vanadium oxide-silica catalyst using a sol-gel method and observed that incorporating small quantities of nitric oxide decreased the energy threshold for H-abstraction, increasing CH_4 conversion and HCHO production. For a 1.5 wt% V content, HCHO selectivity was 32 % due to the presence of V–O–Si species.

Also, for HCHO production from CH_4, SiO_2 supported metal oxides (e.g., VO_x/SiO_2, MoO_x/SiO_2, and FeO_x/SiO_2) have been found to be more suitable than acidic or basic supports (e.g., Al_2O_3, TiO_2, and/or SnO_2). The results have shown that highly dispersed, active metal oxide species are needed for the selective formation of HCHO. If the oxides aggregate, they promote the oxidation of HCHO to CO and CO_2 [1,42].

It is important to note that the high selectivities to HCHO on different metal oxide catalysts can be obtained only at quite low CH_4 conversions (< 2 %) or low O_2/CH_4 ratios (< 0.5) rendering these processes unfeasible for large scale use.

In this context, the primary objective of this study was to create catalytic systems that contain both highly efficient and selective components that can directly oxidize CH_4 to CH_3OH and/or HCHO at low temperatures. Herein, we employed, for the first time, polycrystalline Ti_3SiC_2 MAX phase as support for different MO_x loadings and tested the resulting catalysts in the DOM. The catalysts were prepared using a straightforward and cost-effective hydrothermal, HT, process and were characterized using different techniques.

2. Experimental details

2.1. Catalysts synthesis

The synthesis methodology details of Ti_3SiC_2 can be found published elsewhere [26] and also a short description in Supplementary Information. X-Ray diffraction (XRD) demonstrated the presence of only Ti_3SiC_2 (Fig. SI1). Pure MO_x and MO_x/Ti_3SiC_2 samples with different wt % of MO_x (with 5, 10 and 20 wt%) were synthesized using a hydrothermal method. The synthesis details are summarized in Scheme SI1 and are the following: first, an appropriate amount of a metal precursor, vanadyl acetylacetonate, $VO(acac)_2$, (99 %, Thermo Scientific) and copper nitrate, $Cu(NO_3)_2$•3 H_2O, (≥98 %, Sigma-Aldrich) as the V- and Cu-based precursor, respectively. Powders of the latter were mixed with 45 mL ethanol, EtOH, (absolute, ≥ 99.5 %, Merck) and stirred until complete dissolution. Subsequently, 5 mL of deionized (DI) water was added to the solution and stirred for 30 min. Following that, 0.5 g Ti_3SiC_2 powders were added into the solution and stirred continuously for an additional 30 min. Next, the resulting solution was transferred into a Teflon-lined, stainless-steel autoclave with a capacity of 100 mL and maintained at a temperature of 180 °C for 20 h. Once the synthesized product cooled to room temperature (RT), the resulting solid material was separated by centrifugation and washed with DI water and absolute EtOH. Finally, the obtained powder was dried in air at 200 °C for 5 hours (h). Following this, the dried powder underwent calcination in air at 400 °C for 5 h with a heating rate of 5 °C·min^{-1}. The powders obtained are designated as x%MO_x/Ti_3SiC_2, with MO_x representing either V or Cu oxides, and x corresponding to 5, 10, or 20 wt%. For comparison, a Ti_3SiC_2 powder was also HT treated without the addition of any metal oxides. This batch is henceforth labeled as HT-Ti_3SiC_2. In addition, pure metal oxides powders Cu_2O and V_2O_5 were prepared using the same HT method described above.

2.2. Characterization methods

Structural investigations were performed using a powder X-ray diffraction (XRD) diffractometer (D8 ADVANCE, BRUKER-57AXS GmbH, Germany) with Ni-filtered Cu radiation (λ=1.54184 Å), at RT, in the Bragg-Brentano geometry, in the 2θ range from 9° to 70° at a scanning rate of 0.02 °/min. The Rietveld refinement of the recorded XRD data was performed using the MAUD (Materials Analysis Using Diffraction) version 2.99 software to determine the lattice parameters, the average crystallite size and quantitative identification of the crystalline phases.

The morphology of the samples was investigated using a scanning electron microscope, SEM and the composition by energy dispersive X-ray spectroscopy, EDX, using a Zeiss EVO 50 XVP SEM equipped with a Quantax Bruker 200 system for EDX. Before SEM analysis, all the samples were coated with a thin gold layer.

The Raman spectra of the prepared samples were acquired using a LabRAM HR Evolution spectrometer from Horiba Jobin-Yvon. The spectra were collected in the 50–1600 cm^{-1} range. The spectrometer was equipped with an air-cooled CCD and a He-Ne laser (633 nm). All spectra were recorded at RT using the extended scan mode by averaging 5 iterations with a 30 s acquisition time each and 25 % of the total power of the laser.

The XPS analysis was conducted using the AXIS Ultra DLD spectrometer (Kratos Analytical Ltd. Manchester, UK). The measurements were performed using the following parameters: pressure of 1×10^{-8} Pa

and radiation from a monochromated Al Kα (hν=1486.74 eV) X-ray cannon with a power of 144 W (12 kV×12 mA). To prevent charging effects a charge neutralizer was employed. At the C 1 s line (BE = 284.6 eV, C–C bond) of the adsorbed hydrocarbon on the surface of each sample, calibration was performed. The experimental outcomes were analyzed using the XPST plug-in in Igor Pro8 from Wavemetrics.

Thermogravimetric, TG, analysis was performed on a Themys One 1150 TGA apparatus under O_2 (purity 5.0) atmosphere, from RT up to 600 °C, with a heating rate of 10 °C·min^{-1}.

The reduction behavior of the MO_x/Ti_3SiC_2 system was studied by performing temperature-programmed reduction, TPR, analysis on a 3FLEX apparatus from Micromeritics. The following analysis conditions were used: sample (approx. 0.1 g) was thermally treated at 200 °C under He (20 mL·min^{-1}) for 1 h to clean the surface, then the temperature was decreased to 23 °C and the reduction process started. Here, a flow of 5 v/v% H_2-Ar gas with a rate of 20 mL·min^{-1} was employed, at a heating rate of 10 °C·min^{-1}, until 500 °C is reached.

To determine the total amount of Cu and V, the solid samples were digested in a mixture of **40 vol%** aqueous HCl and HNO_3 and then, for detection of the signal intensity of the copper and vanadium ions, the resulting solutions were introduced into the PlasmaQuant MS Elite ICP-MS (Inductively Coupled Plasma-Mass Spectrometry) system from Analytik Jena AG (Überlingen, Germany) equipped with a double-pass Scott-type spray chamber (Peltier cooled at 3 °C), a concentric glass nebulizer and Cetac ASX-560 (Cetac Technologies, Omaha, NE, USA) autosampler. Calibration solutions were prepared by the dilution of copper and vanadium certified reference materials solution containing 1000 mg L^{-1} of V and 1000 mg L^{-1} of Cu (certified value with an uncertainty of 1000.2 ± 3 mg L^{-1}) purchased from CPA Chem (Stara Zagora, Bulgaria).

2.3. Catalytic tests

The CH_4 oxidation was performed in a fixed-bed quartz tube reactor under atmospheric pressure. Tests were conducted to measure catalytic activity at various reaction temperatures ranging from 250 °C to 400 °C. Prior to the reaction, the catalysts were treated at 400 °C under a flow of N_2 (20 mL·min^{-1}) for 1 h in order to clean their surfaces. The feed gas ratios of CH_4 to O_2, included 1:1, 9:1, and 1:9, respectively. The total flow rate was set to 20 mL·min^{-1}. The balancing gas used in this process was N_2. The catalytic tests were achieved using 100 mg of catalyst, which corresponds to a weight hour space velocity, WHSV, of 12,000 h^{-1}.

3. Results and discussion

3.1. Catalyst characterization

The crystal structures of the as-prepared powders were identified from XRD powder patterns. To test the thermal stability of the Ti_3SiC_2 phase, 0.5 g of powders was HT treated without the metal salts. The XRD patterns for the HT-Ti_3SiC_2 and as- received Ti_3SiC_2 powders are shown in Supplementary Materials, Fig. SI1. The support used, Ti_3SiC_2, presents all diffraction lines corresponding to the Ti_3SiC_2 phase (d = 140.7 ±1.3 nm) according to cif no 1520829 with three additional lines characteristic to TiC (d = 63.7±1.0 nm), according to cif no 9012564. From Rietveld analysis (see Table SI1) we concluded that the TiC phase represents approx. 5 wt% of the support material [43–45]. After heating at 180 °C for 20 h, the HT-Ti_3SiC_2 XRD patterns only changed slightly the intensity of the diffraction lines with the presence of a small quantity, less than 15 wt%, of Ti_3SiC_2 transformed to TiO_2 [46,47], denoting a reasonable stability of the Ti_3SiC_2 phase under HT conditions used here.

The diffractograms of the *x*%VO_x/Ti_3SiC_2 composite powders, and VO_x, are presented in Fig. 1a. The pure VO_x was indexed as orthorhombic V_2O_5 (cif no 2020756), with a crystallite average size of 86.0 ±0.8 nm. By combining the VO_x with the Ti_3SiC_2, five diffraction lines denoted by red lines, are observed at 2θ = 15.34, 20.31, 21.70, 26.16, and 31.03°. These correspond to VO_x lines (compare the red pattern and those above it). The peak at 2θ = 20.31, is noteworthy. Its intensity increases with VO_x content. By increasing the V loading, the intensity of the line at 20.31° 2θ, attributed to the most V_2O_5 intense line - corresponding to the (001) plane - increases. Note that under all conditions, the major peaks belonging to the MAX phase are retained indicating that whatever oxide layer formed it was quite thin and most likely amorphous.

The XRD patterns for CuO_x based samples are shown in Fig. 1b. The pure CuO_x sample was indexed as cubic Cu_2O (cif no 1010941), with a crystallite average size of 172.2±0.2 nm. Here again, all major lines belonging to the MAX phase were retained even after calcination at 400 °C. In this case, however, a peak near 25.3° 2θ, is attributed to TiO_2. All the composite materials present diffraction lines characteristic of Cu_2O

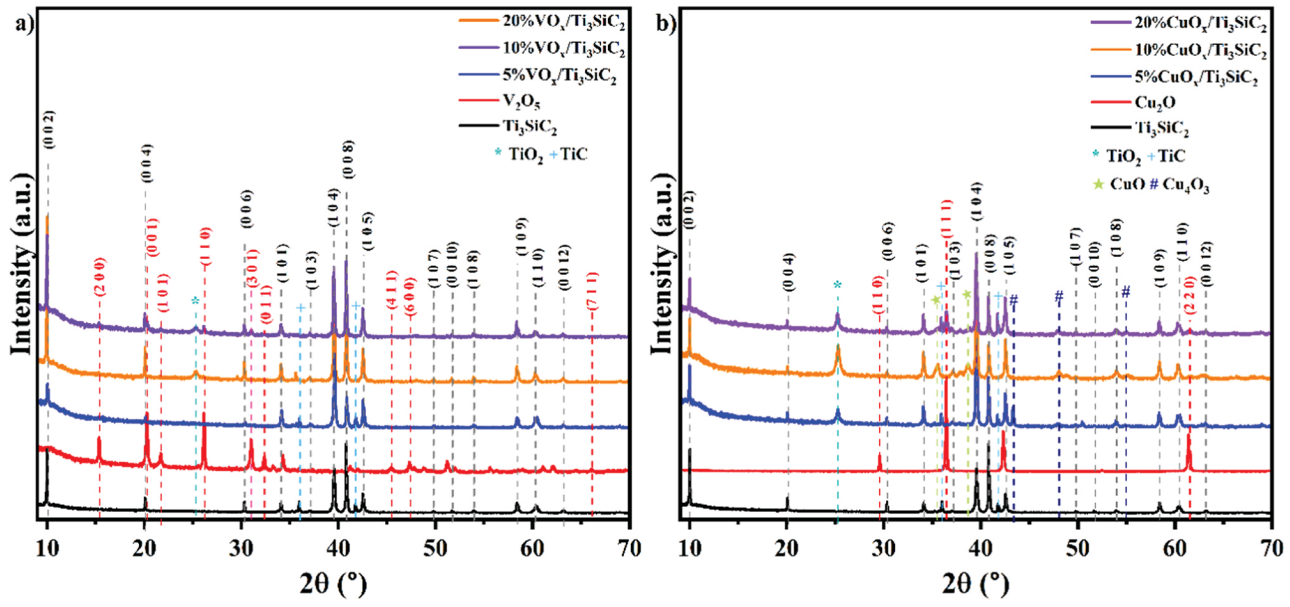

Fig. 1. XRD patterns of, (a) V_2O_5, x%VO_x /Ti_3SiC_2 and (b) Cu_2O, x%CuO_x/Ti_3SiC_2 (where x = 5, 10, and 20 wt% of V or Cu).

indicating the successful deposition of CuO_x on Ti_3SiC_2 with two maxima at $2\theta = 36.67$ and 61.85° (Fig. 1b). As the loading of CuO_x increases, there is a small increase in the peak intensity at 36.67° and 61.85° 2θ, attributed to the (111) and to (220) planes of Cu_2O. However, two low-intensity diffraction lines around 35.5° and 38.7° 2θ attributed to CuO were evidenced in the diffraction patterns.

The formation of Cu_2O rather than CuO was somewhat unexpected since the latter is the stable oxide in air at 1 atm. However, it is consistent with findings observed by others who showed that when thin Cu films were heated in air at temperatures < 300 °C, nanocrystalline Cu_2O was formed [48–50]. As the annealing temperature increased, the most stable CuO phase began to grow [51]. Also, it seems that for particle sizes below 25 nm, the cubic Cu_2O phase is more commonly observed compared to the monoclinic CuO phase obtained after calcination at 400 °C [52].

The morphologies of the various powders synthesized herein can be seen in the SEM micrographs shown in Fig. 2. The Ti_3SiC_2 powder used as a support material (Fig. 2a), is angular and at higher magnifications (not shown) the compact layered structure can be observed. The V_2O_5 nanoparticles (Fig. 2b) are clustered in randomly shaped formations usually with a size below 1 μm. The Cu_2O nanoparticles (Fig. 2c) tend to agglomerate into larger formations (10–20 μm) with relatively uniform morphologies.

In the 20 %VO_x/Ti_3SiC_2 composite samples (Fig. 2d), the layered morphology of the Ti_3SiC_2 powder decorated with VO_x nanoparticles, that are quite well dispersed, can be observed and identified. Similarly, for the 20 %CuO_x/Ti_3SiC_2 sample, the CuO_x nanoparticles can be identified on the surface of the Ti_3SiC_2 support (Fig. 2e), also showing very good dispersion. Higher magnification SEM micrographs that better show the distribution of the Cu and V nanoparticles for the 10 %MO_x/Ti_3SiC_2 samples are presented in Fig. SI2. Deposition of various loadings of VO_x and CuO_x over Ti_3SiC_2 did not affect the compact layered morphology of the support. Also, in Fig. SI2 SEM micrographs of HT-Ti_3SiC_2 sample are presented, indicating that the layered morphology of Ti_3SiC_2 was not affected by the HT treatment.

The EDX results of the synthesized samples are presented in Table SI2. The results obtained should be interpreted mainly qualitatively, due to the X-ray absorption phenomena related to the presence of the Au coating. The quantification data of the lighter elements (C and O) is predominantly affected. However, V and Cu behave predictably in the composite samples, i.e. by increasing the nominal amount of MO_x, there is a concomitant increase in the at% metal supported, V or Cu, but the values are much lower than the theoretical ones. This was also confirmed by the quantitative elemental analysis of V and Cu by ICP-MS. The data are presented in Table SI2. The lower experimental loadings can be explained by the fact that our support used is titanium carbide, specifically Ti_3SiC_2, which doesn't present OH groups on the surface unlike other supports (SiO_2, TiO_2, SnO_2 or Al_2O_3). Therefore, the quantity of V or Cu that binds to the support is lower than the original nominal concentration, which is the case as evidenced by ICP, EDX and XPS data.

Fig. 3a and b plot the Raman spectra of the composite powders, and their metal oxides. The Raman spectra of ternary carbide Ti_3SiC_2 display seven clearly distinguishable modes, specifically $2A_{1\,g}$, $2E_{1\,g}$ and $3E_{2\,g}$. with frequency of 130, 156, 221, 276, 620 and 669 cm^{-1}. The measured modes closely align with the Raman modes predicted by Amer *et al.* through *ab initio* calculation and other published results [53]. The vibrational modes of the C–Ti–Si bonds are responsible for the peaks observed at 221 and 276 cm^{-1}, whereas the Raman shifts at 669 and 620 cm^{-1} can be attributed to the vibration modes of the C–Ti–C bonds.

The Raman spectra of the prepared V- and Cu-based oxides show specific peaks of vibrations characteristic for V_2O_5 and Cu_2O, respectively. Further clarification regarding the identification of these peaks can be found in the SI. Both Raman peaks of vibrations characteristic for Ti_3SiC_2 and V_2O_5 are observed in the spectrum of the x%VO_x/Ti_3SiC_2 composites. In the same time, the spectra obtained for the composite powders exhibit observable Raman shifts characteristic for the Ti_3SiC_2 phase. We cannot exclude the presence of the Cu_2O phase; however, the Raman shifts are superimposing with Raman bands characteristic of the Ti_3SiC_2, phase (the ones around 220, 5210 and 620 cm^{-1}). These observations are consistent with the XRD data of these materials, where low-intensity lines characteristic of Cu_2O are also observed.

High-resolution XPS spectra of some of the materials used here are plotted in Fig. 4 and SI3. The V 2p and Cu 2p are plotted in Fig. 4a and b,

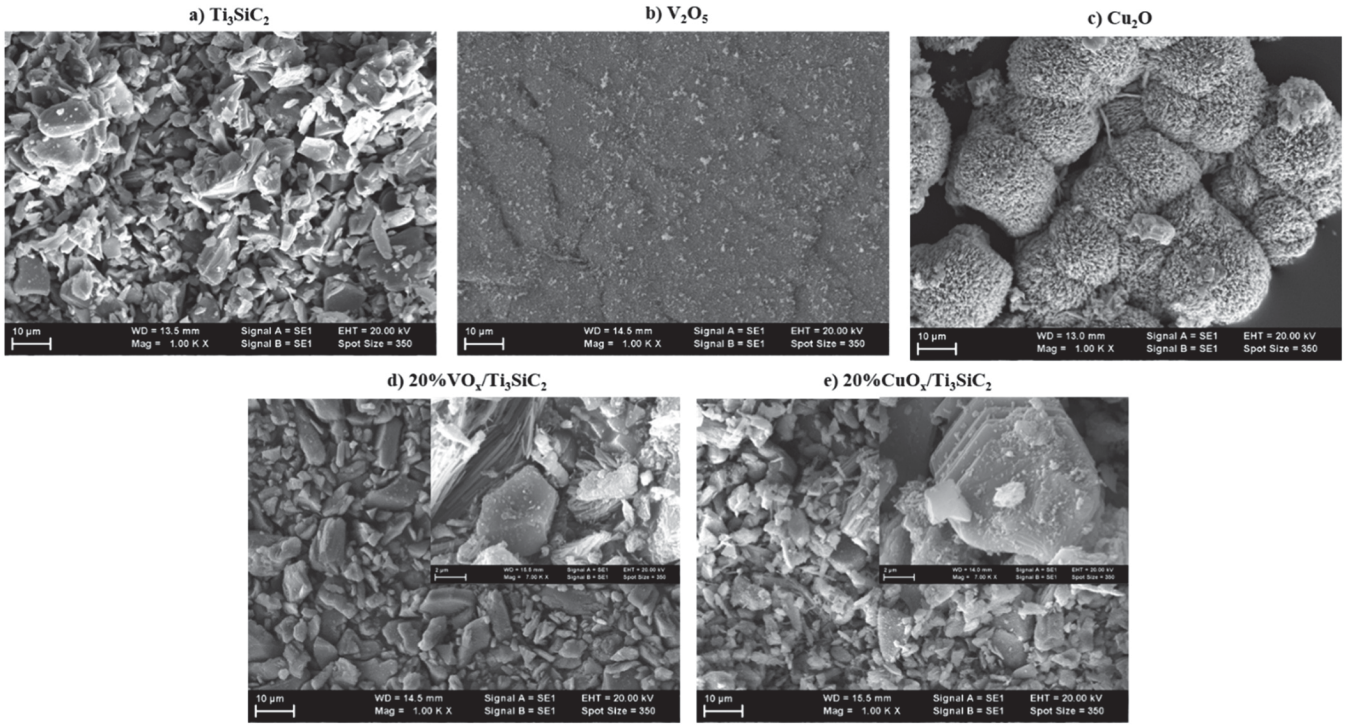

Fig. 2. SEM images for, (a) as-received Ti_3SiC_2, (b) V_2O_5, (c) Cu_2O, (d) 20 %VO_x/Ti_3SiC_2, and (e) 20 %CuO_x/Ti_3SiC_2 samples.

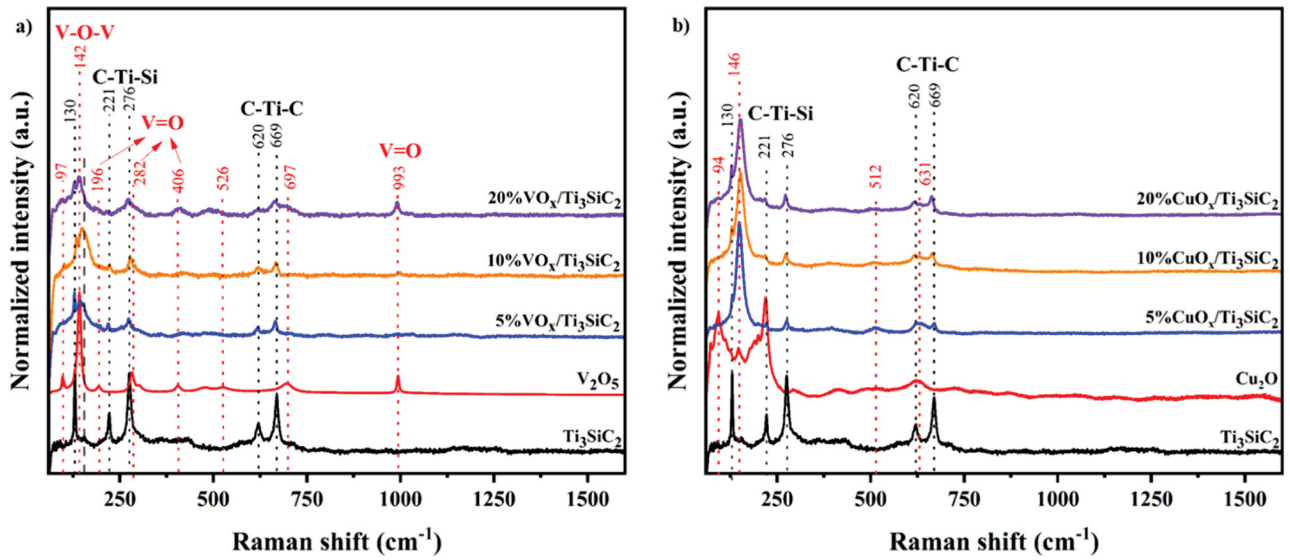

Fig. 3. Raman spectra of Ti_3SiC_2 and composites indicated on panels. (a) VO_x, and (b) CuO_x.

respectively.

When the XPS spectra of the as-received Ti_3SiC_2 powders (not shown) are compared to that of the HT-Ti_3SiC_2 sample no evidence exists for specific Ti–C bonds neither in the C 1 s region ~281–282 eV (Fig. SI3a, b) or in the Ti 2p ~455 eV region (Fig. SI3a and Fig. 4b). The Si signal is also quite low meaning that at the surface an oxidized layer formed during the hydrothermal treatment [35]. For this sample, the C 1 s components identified at the surface are C sp^2 and sp^3 at 284 eV and 285.5 eV, respectively and O–C═O (288.8 eV) due to oxidation or some contamination (carbonate). The Ti $2p_{3/2}$ core-level found at 458.8 eV (Fig. 4b, e) is specific for Ti^{4+}–O bond [35], and the Si 2p at ~102.0 eV (Fig. SI3c) is specific for suboxide SiO_x [54]. Due to the hydrothermal treatment, the ratio of Ti/Si (1.5) is also modified (Table SI3). The O 1 s core-level indicates two main components, one specific of the M–O bond at ~530 eV that can be associated with Ti–O–Ti at the surface, while the peak at ~531.5 eV can be associated with Ti–C–O components [55,56]. The component located at 533.3 eV is specific for the Si–O bond [57] (Fig. 4c).

The binding energies, BEs, of the Ti 2p, C 1s, and O 1 s components remain unchanged after HT addition of VO_x to Ti_3SiC_2, which means that the support structure is similar to that observed on the HT-Ti_3SiC_2 sample. The sole change noticed was in the O 1 s component ratios of the VO_x/Ti_3SiC_2 samples. The component at ~530 eV can be associated with both Ti–O–Ti and V-O bonds. For the 10 %VO_x/Ti_3SiC_2 sample, there was an important increase in the quantity of the Si-O bonds at the surface from 2 % to 12 % (Fig. 4c), meaning that the surface contains more SiO_2 as result of the V loading. Surprisingly, when higher amount of V (20 %) is loaded on the sample, the component at ~530 eV, assigned to Ti-O-Ti and V-O is found as main component, indicating most probably the presence of VO_x onto the surface in higher amounts. In this case, the Si-O component remained in lower amount onto the surface (2 %). As the amount of VO_x increased, the Si 2p BEs shifts toward higher values, suggesting that the oxidation state increased as well (Fig. 4a). The V 2p high resolution spectra denoted the presence of two oxidation states, mainly V^{5+} (517.3 eV) and, to a lesser extent V^{4+} (~516.0 eV) [58]. An increase of the V content resulted in an increase of the V^{5+}/V^{4+} ratio (Table SI3).

The deposition of CuO_x on the Ti_3SiC_2 surfaces resulted in materials with behaviour similar to VO_x/Ti_3SiC_2. The BE of C 1 s component remains unchanged, while the Ti 2p component is slightly shifted (0.2 eV) to lower BEs, most probably to the interaction of Cu with Ti. Adding Cu on Ti_3SiC_2, resulted in an important change in the O 1 s high resolution spectra. A new component at lower binding energies (528.8 eV) appears in the O 1 s core-level when CuO_x is added (Fig. 4f), which can be assigned to the Cu^{2+}–O bond [59], for both samples 10 %CuO_x/Ti_3SiC_2 and 20 %CuO_x/Ti_3SiC_2. In contrast with the V-loaded samples, 10 % CuO_x addition does not change significantly the surface ratio of the O 1 s components, except for the appearance of evidences of existing Cu^{2+}–O bonds. In case of 20 %CuO_x/Ti_3SiC_2 sample, SiO_2 can be found in higher amounts, sustaining the formation of a superficial oxide layer. Regarding the oxidation state of Cu, we cannot use the XPS analysis as evidence since the Cu_2O is oxidised to CuO under the X-ray beam, a phenomenon acknowledged by the scientific community [60]. Indeed, the Cu 2p spectrum from Fig. 4d points out to the existence on the surface of CuO, due to the presence of satellite peaks located in the 940–950 eV range [61]. However, from TPR profile (Fig. SI4) and XRD we cannot exclude the presence of CuO on the surface but in very small amounts.

The XPS analysis for 10 %VO_x/Ti_3SiC_2 after the reaction preserved the components detected before reaction (Fig. SI3). Due to the reductive atmosphere (CH_4) during reaction, a slight reduction of Ti 2p with 0.3 eV, reduction of V^{5+} to V^{4+}, and reduction of M–O component from O 1 s were observed. Si 2p spectra highlight oxidation of SiO_x component (102.8 eV). This is an interesting observation showing that, under a mixture of CH_4 and O_2 flow, the Ti^{4+} and V^{5+} cations are reduced by the CH_4 atmosphere, while Si is oxidised in the mixture flow. Additionally, from the O 1s spectra we observed that Ti–C–O component increases after testing (Fig. SI3). Similar behaviour was observed by Wesley *et al.* [33] on MAX phase, Ti_3AlC_2, surface when it was used as catalyst for oxidative dehydrogenation of *n*-butane. They claimed that the adsorbed oxygen species formed upon activation of gas-phase O_2 can activate *n*-butane dehydrogenation.

The TG technique under an oxygen atmosphere was employed to determine the oxidation stability of Ti_3SiC_2, 20 %CuO_x/Ti_3SiC_2 and 20 %VO_x/Ti_3SiC_2 powders. The results are presented in Fig. 5. In the RT–200 °C region (Fig. 5a), Ti_3SiC_2 is quite inert, exhibiting a small reduction in mass at around 200 °C that can most probably be attributed to the evaporation of adsorbed water. In the 200–400 °C temperature range, the Ti_3SiC_2 powders are also quite inert as found in previous work [62]. Beyond 400 °C, there is a modest 12 % increase in mass, indicating the initiation of oxidation.

The TG response of the 20 %CuO_x/Ti_3SiC_2 and 20 %VO_x/Ti_3SiC_2 powders, shown in Fig. 5b and c, respectively, are quite comparable to that of the pure Ti_3SiC_2 powder. The small reduction in mass at 200 °C was no longer evident. Both samples exhibited excellent oxidation stability up to 350 °C. Beyond 350 °C, there was mass uptake up to 600 °C

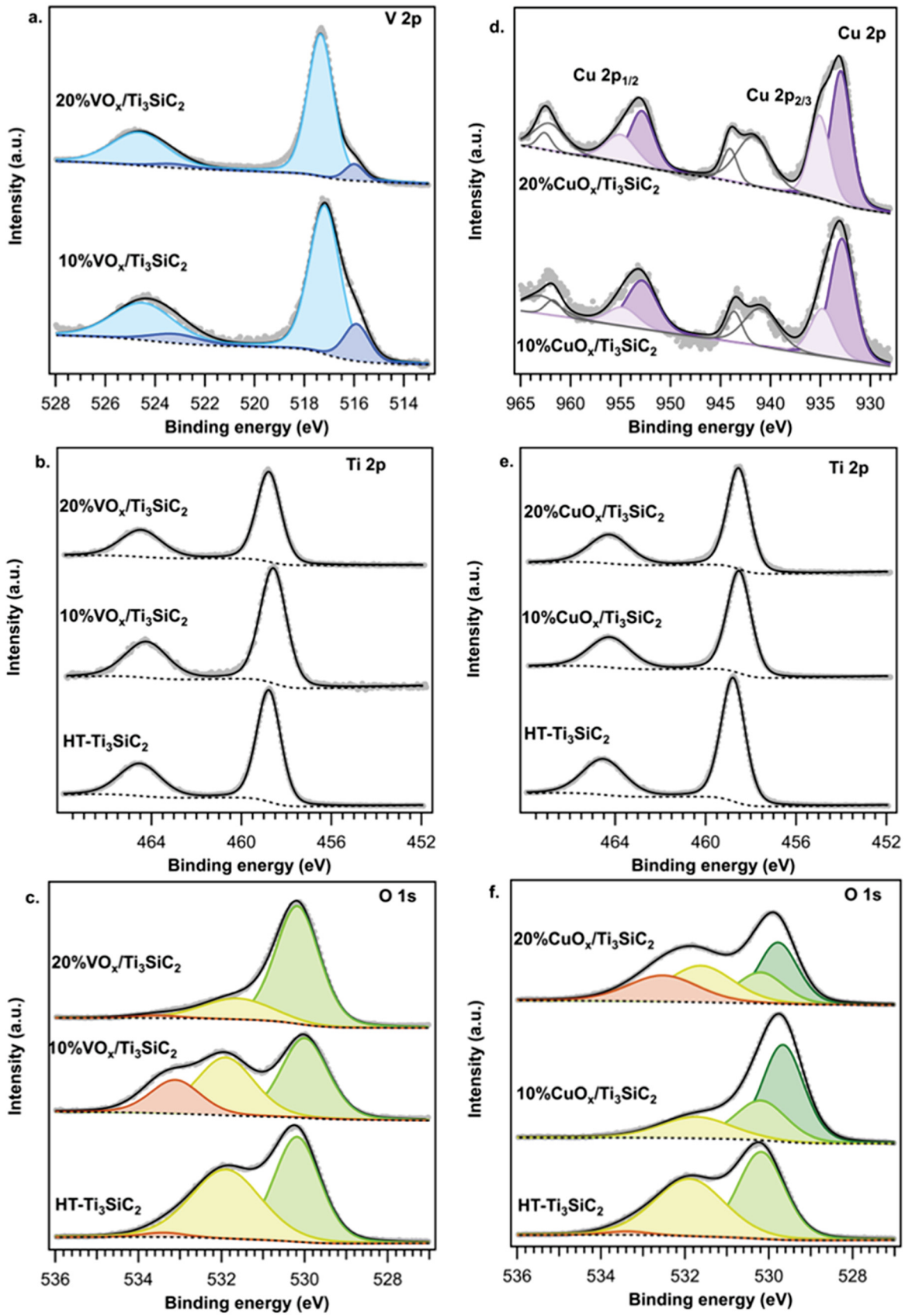

Fig. 4. XPS high resolution spectra for, (a) V 2p, (b) Ti 2p and (c) O 1 s in x%VO_x/Ti_3SiC_2, and (d) Cu 2p, (e) Ti 2p and (f) O 1 s in x%CuO_x/Ti_3SiC_2.

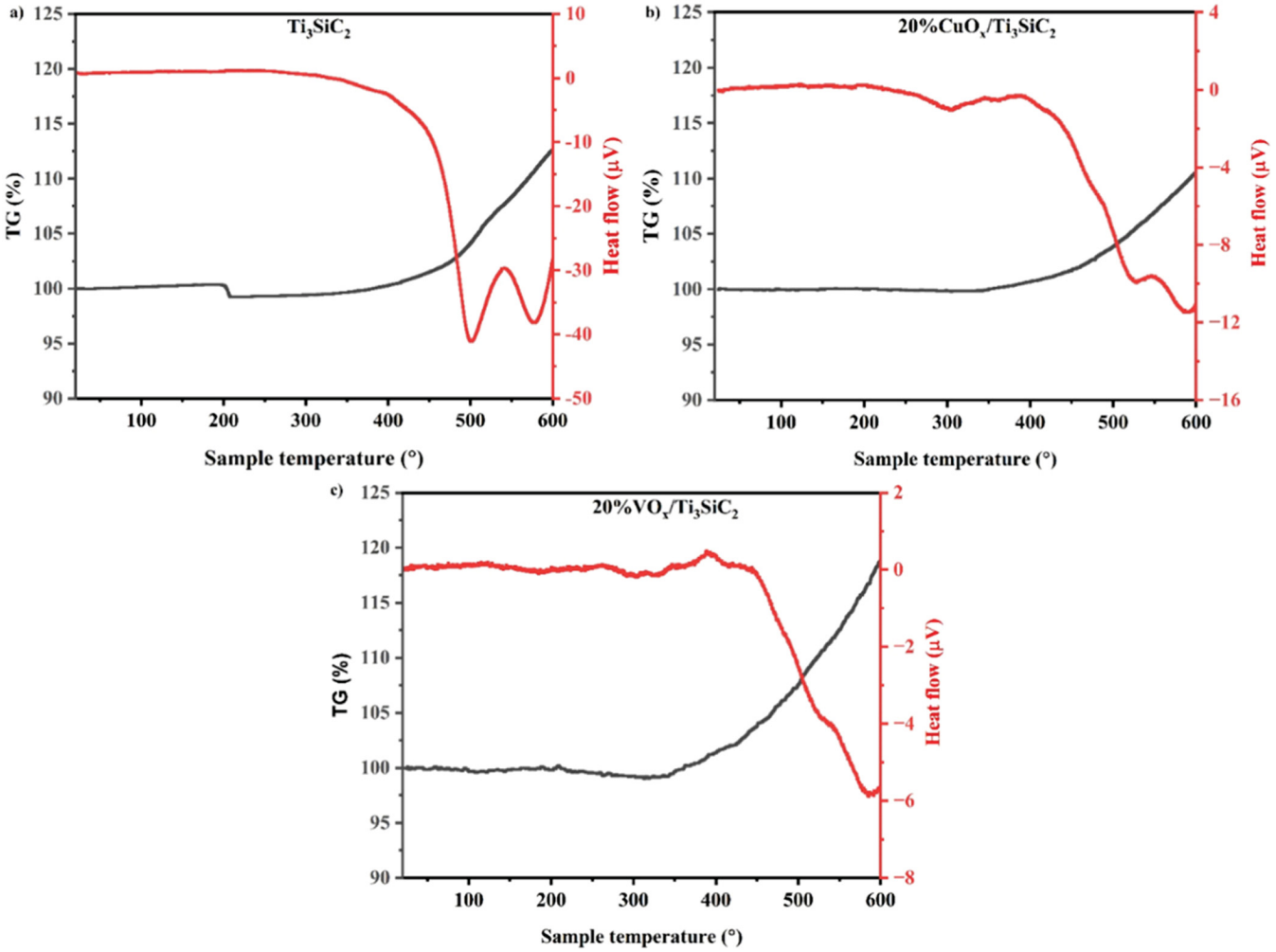

Fig. 5. TG analysis of, (a) Ti_3SiC_2, (b) 20 $\%CuO_x/Ti_3SiC_2$, and (c) 20 $\%VO_x/Ti_3SiC_2$ powders under O_2 atmosphere.

which corresponded to surface oxidation, in agreement with data obtained in XPS.

The small exothermic peaks observed at 525 and 590 °C in Figs. 5b and 5c, respectively, most probably correspond to the formation of TiO_2 [63].

The H_2-TPR profiles for the $x\%CuO_x/Ti_3SiC_2$ and $x\%VO_x/Ti_3SiC_2$

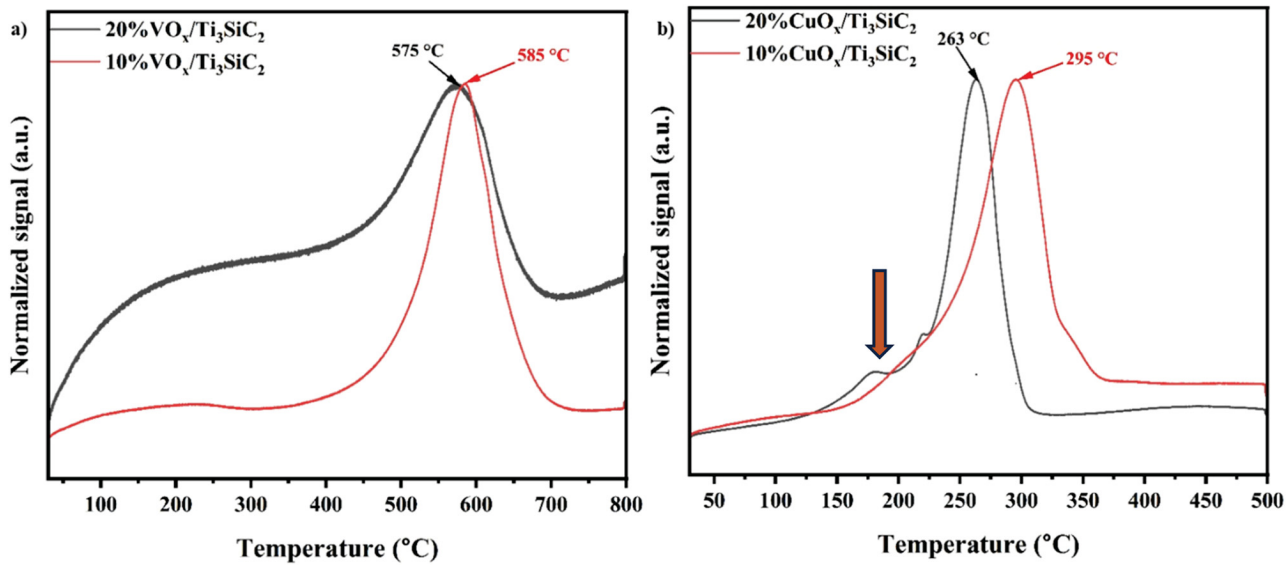

Fig. 6. TPR- H_2 results of, (a) $x\%VO_x/Ti_3SiC_2$ and (b) $x\%CuO_x/Ti_3SiC_2$ catalysts (x=10, 20).

samples (x=10, 20) are presented in Fig. 6. For the V- based powders the reduction process takes place in a wide temperature range with no well-defined peaks below 500 °C which, in agreement with the literature data, indicates that we do not have a highly dispersed monomeric species formed when VO_x was deposited on the Ti_3SiC_2 [40]. At higher temperatures, a wide reduction peak appears at around 580 °C (see Fig. 6a) and can be assigned to the reduction of V in polymeric and bulk like V_2O_5 species [64,65], in good agreement with XRD, Raman and XPS data.

The TPR profiles of the Cu-based samples (Fig. 6b) exhibit reduction peaks at lower temperatures, with maxima at 295 and 263 °C, for the 10 and 20 % CuO_x samples, respectively. The shoulder (noted with an arrow) at lower temperatures can be assigned to the reduction of Cu^{2+} to Cu^{1+} which can be an indication of the presence of Cu^{2+} in very low amounts [66] and maybe this is why was not identified by Raman spectroscopy. The unexpected shift in reduction temperature for the sample containing 10 % CuO_x to higher temperature may be explained by a stronger metal–support interaction between dispersed CuO_x species and the support [67] or bigger particle sizes of the CuO_x clusters.

3.2. Catalytic studies

During this study, we considered the following parameters to find an optimized reaction process for the direct oxidation of CH_4 to CH_3OH and/or HCHO: *i)* reaction temperature (300–400 °C), and *ii)* feed gas ratio between CH_4 and O_2 that varied between 1:1; 1:9 and 9:1, respectively.

In general, the catalytic selective oxidation of CH_4 was realized by O_2 in a continuous flow reactor at ambient pressures. The catalytic contributions from the empty reactor and the pure Ti_3SiC_2 support were found negligible for CH_4 conversion in the reaction conditions employed here. For the prepared catalysts, the reaction products identified by the online GC analysis were HCHO and CO_2. No evidence for the production of CH_3OH, or others C-containing products, was found. However, methanol formation cannot be excluded, since HCHO can be formed by the oxidation of CH_3OH [68].

Selective oxidation of CH_4 is highly exothermic and homogeneous gas phase reactions may contribute to the overall partial oxidation reactions once the reactions are initiated [69]. This can be more favorable at short contact times [70], which is why we performed the reactions at longer contact times relative to the weight of the catalyst and the gas flow rate of 0.3 s^{-1} which corresponds to a WHSV of 12,000 h^{-1}, to avoid autocatalytic reactions and also diffusion limitations. Said otherwise, we used this high reactant WHSV to favor the desorption of formaldehyde from the reaction zone without it being further oxidized.

The temperature dependencies of the CH_4 and O_2 conversions and product selectivities are summarized in Fig. 7. The Ti_3SiC_2 support was tested by itself, but did not present any catalytic activity. The samples with 5 % MO_x were not active in the temperature domain and reaction conditions used here. There are reports in the literature for low-content V-based catalysts being active, but that is only true at much higher temperatures. For instance, a 5 wt% V_2O_5/SiO_2 catalyst was active at 630 °C [13,70]. The maximum temperature used in this study is 400 °C, because the support starts oxidizing at temperatures > 400 °C (see Fig. 5).

Based on the results shown in Fig. 7, we conclude that, in terms of conversion and selectivity to HCOH, the best results were obtained on the CuO_x-based catalysts irrespective of the temperature at DOM was performed. These results are in line with the study of Otsuka and Hatano [71] that established a relationship between conversion and selectivity and cation electronegativity. The electronegativity has a role in the relative rates of the initial H abstraction from CH_4, and oxygen insertion to form formaldehyde. In our case, the conversion increases with increasing electronegativity, and may be an explanation for the fact that Cu is more active knowing that Cu has an electronegativity of 1.9, while V's is 1.65.

These findings are consistent with the TPR profiles that show that the Cu-based samples resulted in significantly lower temperature reduction peaks than the V-containing ones (compare Fig. 6a and b). This is why the Cu-based samples can activate CH_4 at such low temperatures. The reduction temperature of the 20 wt% CuO_x sample is the lowest.

On the other hand, based on the TPR results, we can explain the low CH_4 conversions obtained on the VO_x-based catalysts since no reduction peak was evidenced at low temperatures (see Fig. 6a). The tests performed in the presence of V_2O_5 did not present any selectivity and the conversion was also quite low (traces). However, we can observe that the selectivity level is high for all the supported samples, indicating that the support plays an important role. An explanation is the presence of the superficial oxide layer formed during the HT treatment that covers Ti_3SiC_2, as evidenced by XPS and XRD analysis, in which most probably the O species possess higher mobility than in classical oxide supports. Such behavior, of the Ti_3AlC_2 MAX phase, was also observed by Wesley *et al.* [33] who evidenced the formation of an oxide surface layer containing O-active sites, which was key in the oxidative dehydrogenation of *n*-butane reactions. Taking into account that Ti_3SiC_2 is not active for DOM and the single oxides are not selective, but both, CuO_x and VO_x

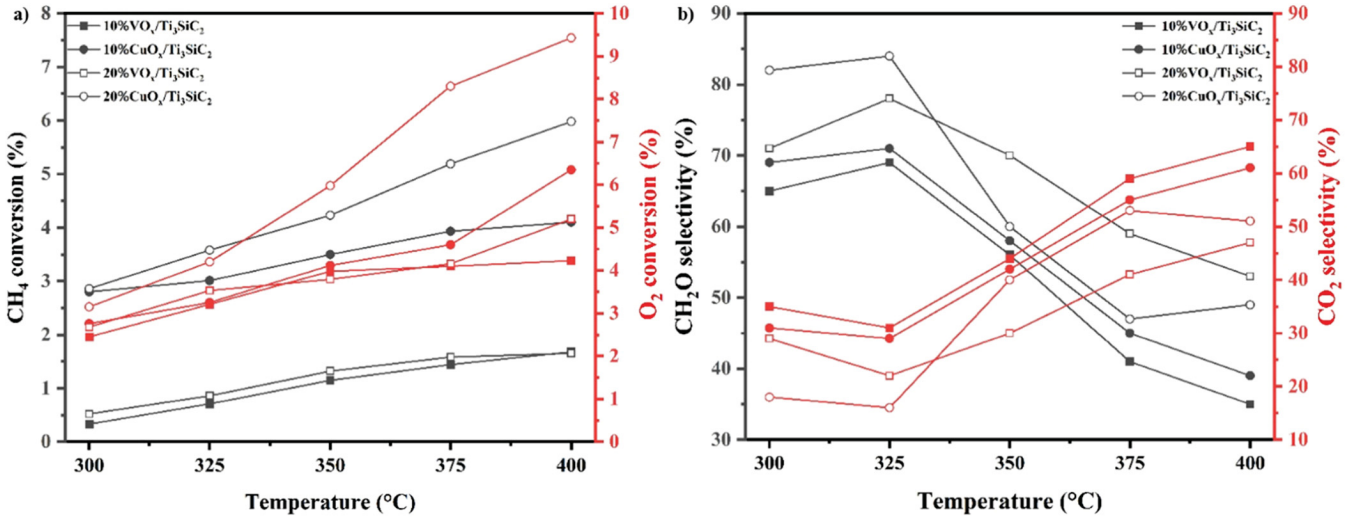

Fig. 7. (a) CH_4 and O_2 conversions, and (b) selectivities to reaction products on different MO_x/Ti_3SiC_2 catalyst powders. Data points and lines are color coded with the left (black) and right (red) y-axes.

supported samples are active and selective, indicates a synergy between the MO_x and the support. We hypothesize that the first reaction step is the adsorption of CH_4 onto the MO_x surface, followed by the extraction of hydrogen atoms and their transfer to Ti_3SiC_2 surface oxygens. In the next step, when HCHO desorbs from the catalyst surface using surface O atoms, resulting in an oxygen defect site, most probably oxygen vacancies. The latter are most probably oxidized by the O_2 from the gaseous phase. This is supported by the XPS data in which the reduction Ti^{4+} to Ti^{3+} was evidenced for the sample upon test, while Si 2p spectra highlight an oxidation and the apparition of a SiO_x component. More studies are needed to prove this hypothesis, however.

This pathway was also suggested by other studies [72] where the intermediate CH_3 and CH_3O surface species formed on metal oxides could be easily attacked by active surface oxygen species generated in the fast dissociative adsorption of oxygen, thus favoring the formation of formaldehyde (and CO_x) over methanol.

The most active sample is 20 %CuO_x/Ti_3SiC_2 for which we succeeded in having a conversion of almost 4 % and a selectivity to HCHO of 84 % at 325 °C under ambient pressure. To appreciate these numbers, it is instructive to compare them with some literature data presented in Table 1. Consistent with our results, the Cu-based samples are more active and selective than the ones containing V. Furthermore, using Ti_3SiC_2 as a support we succeeded to obtain higher selectivities to HCHO at significantly lower temperatures on samples containing Cu. The capability of Cu-containing catalysts was also observed on Cu-zeolite systems that were able to convert CH_4 selectively into CH_3OH at RT indicating that they may also contain highly activated oxygen species [36].

Fig. 8 plots the evolution of HCHO with CH_4 conversion for the 20 % CuO_x/Ti_3SiC_2 catalysts, where it is obvious that HCHO selectivity drops with increasing CH_4 conversion levels (Fig. 8b), which is well recognized in the literature [81]. The same is true of the V-containing system (Fig. 8a).

In accordance with the literature, high selectivity to HCHO was mostly obtained at low CH_4 conversions and CH_4/O_2 ratios of 1 for our MO_x/Ti_3SiC_2 phases. This evolution in HCHO selectivity indicates it is a primary product formed during CH_4 conversion. It has been postulated that the initial activation of CH_4 takes place through active O species from the oxide surfaces that form bonded methoxy intermediates (CH_3O—) via cleaving a C–H bond in CH_4, which undergoes further dehydrogenation to form HCHO [82,83]. In our case, we have small MO_x particles that are well distributed on the Ti_3SiC_2 surfaces (see SEM images, Fig. SI2), and by synergic effects generate more active O species that can activate CH_4. In the case of 20 %CuO_x/Ti_3SiC_2 we obtained a conversion of almost 6 % at 400 °C.

Noteworthily at each temperature, the high HCHO selectivity was only obtained after about ≈ 2 h (Fig. SI4). This can be considered an induction period, in which conversion was quite constant, as HCHO selectivity increased progressively (Fig. SI4). An explanation for this behavior can be related to the surface evolution of the MO_x/Ti_3SiC_2 catalyst which changes slightly during the first period of the reaction as the XPS analysis and XRD data of the tested catalysts show (see Fig. SI3 and Fig. SI5). The induction period was also observed on Pt catalysts during which oxygenated intermediates, such as methanol, acetone, methyl methoxy acetate were detected [84].

In order to explore the influence of the CH_4/O_2 ratio, we performed DOM on 20 %CuO_x/Ti_3SiC_2 at 325 °C in CH_4-rich conditions (CH_4:O_2 = 9:1) to prevent overoxidation of the highly reactive CH_3OH and HCHO reaction products, as well as in O_2 rich conditions (CH_4:O_2 = 1:9) for the same WHSV. The catalytic results are shown in Fig. SI6. A variation in the CH_4 conversion and HCHO selectivity was observed by modifying the CH_4/O_2 ratio; however, the selectivity remained quite high for this temperature. Methane oxidation rates increased with a decrease in the CH_4/O_2 ratio, indicating a positive reaction order concerning O_2. Note our results are different from typical catalysts that use traditional metal oxides as support and that require higher temperatures and pressures to transform CH_4 selectively [85,86]. Working in O_2 rich conditions (CH_4:O_2 = 1:9), the conversion of CH_4 attained was ≈ 4 % while the HCHO selectivity decreased to 69 %. This can be a consequence of the degree of oxidation of the Ti_3SiC_2 surfaces, without any evidence at this moment; more studies need to be performed to understand this behavior.

4. Conclusions

Different CuO_x and VO_x oxides were deposited on Ti_3SiC_2 powders using a straightforward hydrothermal method and tested for DOM to formaldehyde for the first time under atmospheric pressure. The best performance – of almost 4 % CH_4 conversion and 84 % HCHO selectivity- was obtained with CuO_x which was quite active at 325 °C and ambient pressure. This activity is correlated with the low-temperature reduction profile as evidenced by this CuO_x-based material. Our results indicate that the MAX phases in general, and Ti_3SiC_2 in particular, have great potential for designing innovative catalytic processes and can play an important role in the selectivity toward HCHO, by creating a synergy with various MO_x, generating catalysts that are active for the oxidation of CH_4.

CRediT authorship contribution statement

Iuliana M. Chirica: Investigation, Data curation. **Florentina Neatu:** Investigation, Formal analysis, Data curation. **Toton Haldar:** Investigation. **Alexandra Corina Iacoban:** Writing – original draft, Methodology, Investigation, Formal analysis, Data curation. **Mihaela Florea:** Writing – review & editing, Writing – original draft, Project

Table 1
Summary of literature data for CH_4 conversion and our results.

Catalysts	Temp. (C)	O_2/CH_4 ratio	CH_4 conversion (%)	Carbon selectivity (%)				Ref.
				HCHO	CH_3OH	CO	CO_2	
VO_x/SiO_2	650	0.5	13.5	35	-	51	14	[73]
VOx/SBA−15	600	0.13	1.8	36.4	0.8	58.7	4.5	[74]
VO_x/SiO_2	650	0.11	4.5	32.0	-	57.0	11.0	[41]
VOx/MCM−41	650	0.13	5.4	22.0	0.2	-	-	[75]
VO_x/SiO_2	590	0.5	0.9	41	-	59	0	[1]
VO_x/SiO_2	650	0.5	4.6	32.2	-	60	7.8	[41]
VO_x/TiO_2	650	0.5	9.7	2	-	76	22	[42]
CuOx/SBA−15	625	1.00	2.8	44.0	-	28.0	28.0	[76]
CuOx/SBA−15-gra	625	1	2.4	36	-	13	51	[77]
CuFe0.5/2.5-B4	630	0.4*	1.5	71.8	9.1	19.1	0	[78]
Cu-Fe-ZnO	650	1.0	0.2	18	-	82	-	[79]
Cu-MoO_x	700	1	0.4	78	-	14	8	[80]
20 %CuOx/ Ti_3SiC_2	325	1.0	3.58	84	-	-	16	This work
20 %VO_x/ Ti_3SiC_2	325	1.0	0.86	71	-	-	29	This work

* CH_4:N_2O.

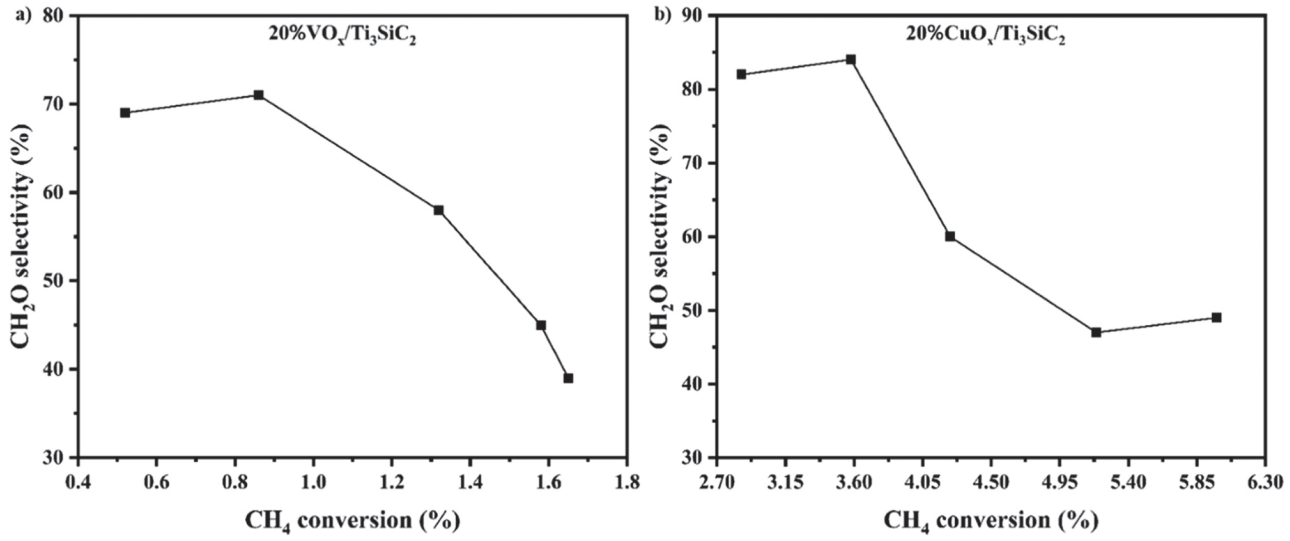

Fig. 8. Formaldehyde selectivity vs. CH_4 conversion over, (a) 20 %VO_x/Ti_3SiC_2, and (b) 20 %CuO_x/Ti_3SiC_2 powders for temperatures of 300, 325, 350, 375 and 400 °C.

administration, Data curation, Conceptualization. **Michel W. Barsoum:** Writing – review & editing, Writing – original draft. **Stefan Neatu:** Investigation, Formal analysis, Data curation. **Anca G. Mirea:** Investigation, Formal analysis, Data curation.

Declaration of Competing Interest

The authors declare that they have no known competing financial interests or personal relationships that could have appeared to influence the work reported in this paper.

Data availability

Data will be made available on request.

Acknowledgements

This work was supported by grants of the Ministry of Research, Innovation and Digitization, CNCS – UEFISCDI, project number PN–III–P4-PCE-2021-1461 and PN–III–P4-ID-ERC-2021-0007, all within PNCDI III. Financial support from Romanian Ministry of Research, Innovation and Digitization through the Core Program 2023–2026 (contract PC3-PN23080303) is gratefully acknowledged. This work was also supported by NSF (DMR-2211319).

Appendix A. Supporting information

Supplementary data associated with this article can be found in the online version at doi:10.1016/j.cattod.2024.114959.

References

[1] K. Shimura, T. Fujitani, Effects of promoters on the performance of a VO_x/SiO_2 catalyst for the oxidation of methane to formaldehyde, Appl. Catal. A Gen. 577 (2019) 44–51.
[2] R. Horn, R. Schlögl, Methane activation by heterogeneous catalysis, Catal. Lett. 145 (2015) 23–39, https://doi.org/10.1007/s10562-014-1417-z.
[3] J.F. Hartwig, Evolution of C-H bond functionalization from methane to methodology, J. Am. Chem. Soc. 138 (2016) 2–24, https://doi.org/10.1021/jacs.5b08707.
[4] M.A. Banares, J.L.G. Fierro, J.B. Moffat, The partial oxidation of methane on MoO3/SiO2 catalysts: influence of the molybdenum content and type of oxidant, J. Catal. 142 (1993) 406–417.
[5] H.D. Gesser, N.R. Hunter, C.B. Prakash, The direct conversion of methane to methanol by controlled oxidation, Chem. Rev. 85 (1985) 235–244, https://doi.org/10.1021/cr00068a001.
[6] C. Hammond, S. Conrad, I. Hermans, Oxidative methane upgrading, ChemSusChem 5 (2012) 1668–1686, https://doi.org/10.1002/cssc.201200299.
[7] T. Zimmermann, M. Soorholtz, M. Bilke, F. Schüth, Selective methane oxidation catalyzed by platinum salts in oleum at turnover frequencies of large-scale industrial processes, J. Am. Chem. Soc. 138 (2016) 12395–12400, https://doi.org/10.1021/jacs.6b05167.
[8] Y. Xi, A. Heyden, Direct oxidation of methane to methanol enabled by electronic atomic monolayer–metal support interaction, ACS Catal. 9 (2019) 6073–6079, https://doi.org/10.1021/acscatal.9b01619.
[9] H. Schwarz, Chemistry with methane: concepts rather than recipes, Angew. Chem. Int. Ed. 50 (2011) 10096–10115, https://doi.org/10.1002/anie.201006424.
[10] D.M. Newitt, P. Szego, Slow oxidations at high pressures I—methane and ethane, II—Methyl alcohol, ethyl alcohol, acetaldehyde, and acetic acid, Proc. R. Soc. Lond. Ser. A-Math. Phys. Sci. 147 (1934) 555–571.
[11] V.S. Arutyunov, The role of pressure in partial oxidation of methane, Russ. Chem. Bull. 51 (2002) 2170–2175, https://doi.org/10.1023/A:1022114830675.
[12] H. Arakawa, M. Aresta, J.N. Armor, M.A. Barteau, E.J. Beckman, A.T. Bell, J. E. Bercaw, C. Creutz, E. Dinjus, D.A. Dixon, K. Domen, D.L. DuBois, J. Eckert, E. Fujita, D.H. Gibson, W.A. Goddard, D.W. Goodman, J. Keller, G.J. Kubas, H. H. Kung, J.E. Lyons, L.E. Manzer, T.J. Marks, K. Morokuma, K.M. Nicholas, R. Periana, L. Que, J. Rostrup-Nielson, W.M.H. Sachtler, L.D. Schmidt, A. Sen, G. A. Somorjai, P.C. Stair, B.R. Stults, W. Tumas, Catalysis research of relevance to carbon management: progress, challenges, and opportunities, Chem. Rev. 101 (2001) 953–996, https://doi.org/10.1021/cr000018s.
[13] M. Ravi, M. Ranocchiari, J.A. vanBokhoven, The direct catalytic oxidation of methane to methanol—a critical assessment, Angew. Chem. Int. Ed. 56 (2017) 16464–16483, https://doi.org/10.1002/anie.201702550.
[14] T.V. Choudhary, V.R. Choudhary, Energy-efficient syngas production through catalytic oxy-methane reforming reactions, Angew. Chem. Int. Ed. 47 (2008) 1828–1847, https://doi.org/10.1002/anie.200701237.
[15] N.F. Goldshleger, M.B. Tyabin, A.E. Shilov, A.A. Shteinman, Activation of saturated hydrocarbons-deuterium-hydrogen exchange in solutions of transition metal complexes, Russ. J. Phys. Chem. 43 (1969) 1222.
[16] B.G. Hashiguchi, M.M. Konnick, S.M. Bischof, S.J. Gustafson, D. Devarajan, N. Gunsalus, D.H. Ess, R.A. Periana, Main-group compounds selectively oxidize mixtures of methane, ethane, and propane to alcohol Esters, Science 343 (80) (2014) 1232–1237, https://doi.org/10.1126/science.1249357.
[17] R.A. Periana, D.J. Taube, S. Gamble, H. Taube, T. Satoh, H. Fujii, Platinum catalysts for the high-yield oxidation of methane to a methanol derivative, Science 280 (80) (1998) 560–564, https://doi.org/10.1126/science.280.5363.560.
[18] S.J. Tauster, Strong metal-support interactions, Acc. Chem. Res. 20 (1987) 389–394.
[19] S.J. Tauster, S.C. Fung, R.L. Garten, Strong metal-support interactions. Group 8 noble metals supported on titanium dioxide, J. Am. Chem. Soc. 100 (1978) 170–175.
[20] H.R. Sadeghi, V.E. Henrich, SMSI in Rh/TiO_2 model catalysts: evidence for oxide migration, J. Catal. 87 (1984) 279–282.
[21] H.R. Sadeghi, V.E. Henrich, Rh on TiO/sub$_2$: model catalyst studies of the strong metal-support interaction, Appl. Surf. Sci. 19 (1984).
[22] D.N. Belton, Y.M. Sun, J.M. White, Metal-support interactions on rhodium and platinum/titanium dioxide model catalysts, J. Phys. Chem. 88 (1984) 5172–5176.
[23] A.J. Simoens, R.T.K. Baker, D.J. Dwyer, C.R.F. Lund, R.J. Madon, A study of the nickel-titanium oxide interaction, J. Catal. 86 (1984) 359–372.
[24] G.-M. Schwab, in: D.D. Eley, H. Pines, P.B.B.T.-A. in C. Weisz (Eds.), Electronics of Supported Catalysts, , Academic Press, 1979, pp. 1–22, https://doi.org/10.1016/S0360-0564(08)60052-8.

[25] V.H. Nowotny, Strukturchemie einiger Verbindungen der Übergangsmetalle mit den elementen C, Si, Ge, Sn, Prog. Solid State Chem. 5 (1971) 27–70, https://doi.org/10.1016/0079-6786(71)90016-1.

[26] M.W. Barsoum, T. El-Raghy, Synthesis and characterization of a remarkable ceramic: Ti3SiC2, J. Am. Ceram. Soc. 79 (1996) 1953–1956.

[27] M.W. Barsoum, The MN+1AXN phases: a new class of solids: Thermodynamically stable nanolaminates, Prog. Solid State Chem. 28 (2000) 201–281, https://doi.org/10.1016/S0079-6786(00)00006-6.

[28] Z.M. Sun, H. Hashimoto, Z.F. Zhang, S.L. Yang, S. Tada, Synthesis and characterization of a metallic ceramic material–Ti3SiC2, Mater. Trans. 47 (2006) 170–174.

[29] M. Dahlqvist, M.W. Barsoum, J. Rosen, MAX phases – Past, present, and future, Mater. Today 72 (2024) 1–24, https://doi.org/10.1016/j.mattod.2023.11.010.

[30] M.W. Barsoum, M. Radovic, Elastic and Mechanical Properties of the MAX Phases, Annu. Rev. Mater. Res. 41 (2011) 195–227, https://doi.org/10.1146/annurev-matsci-062910-100448.

[31] M.W. Barsoum, MAX Phases: Properties of Machinable Ternary Carbides and Nitrides, Wiley-VCH Verlag, 2013.

[32] M.W. Barsoum, T. El-Raghy, The MAX phases: unique new carbide and nitride materials: ternary ceramics turn out to be surprisingly soft and machinable, yet also heat-tolerant, strong and lightweight, Am. Sci. 89 (2001) 334–343.

[33] W.H.K. Ng, E.S. Gnanakumar, E. Batyrev, S.K. Sharma, P.K. Pujari, H.F. Greer, W. Zhou, R. Sakidja, G. Rothenberg, M.W. Barsoum, N.R. Shiju, The Ti3AlC2 MAX phase as an efficient catalyst for oxidative dehydrogenation of n-Butane, Angew. Chem. Int. Ed. 57 (2018) 1485–1490, https://doi.org/10.1002/anie.201702196.

[34] M.M. Trandafir, F. Neaţu, I.M. Chirica, A.C. Neaţu, E.I. Kuncser, V. Cucolea, M. W. Natu, M. Barsoum, Florea, Highly efficient ultralow Pd loading supported on MAX phases for chemoselective hydrogenation, ACS Catal. 10 (2020) 5899–5908, https://doi.org/10.1021/acscatal.0c00082.

[35] E.H. Kisi, J.A.A. Crossley, S. Myhra, M.W. Barsoum, Structure and crystal chemistry of Ti3SiC2, J. Phys. Chem. Solids 59 (1998) 1437–1443, https://doi.org/10.1016/S0022-3697(98)00226-1.

[36] M.H. Groothaert, P.J. Smeets, B.F. Sels, P.A. Jacobs, R.A. Schoonheydt, Selective oxidation of methane by the bis (μ-oxo) dicopper core stabilized on ZSM-5 and mordenite zeolites, J. Am. Chem. Soc. 127 (2005) 1394–1395.

[37] Y. Li, S. Chen, Q. Zhang, Y. Wang, Copper-catalyzed selective oxidation of methane to formaldehyde by oxygen, Chem. Lett. 35 (2006) 572–573.

[38] G. Águila, F. Gracia, J. Cortés, P. Araya, Effect of copper species and the presence of reaction products on the activity of methane oxidation on supported CuO catalysts, Appl. Catal. B Environ. 77 (2008) 325–338.

[39] H. Launay, S. Loridant, A. Pigamo, J.L. Dubois, J.M.M. Millet, Vanadium species in new catalysts for the selective oxidation of methane to formaldehyde: specificity and molecular structure dynamics with water, J. Catal. 246 (2007) 390–398, https://doi.org/10.1016/j.jcat.2007.01.004.

[40] E. Yang, J.G. Lee, D.H. Kim, Y.S. Jung, J.H. Kwak, E.D. Park, K. An, SiO2@V2O5@Al2O3 core–shell catalysts with high activity and stability for methane oxidation to formaldehyde, J. Catal. 368 (2018) 134–144, https://doi.org/10.1016/j.jcat.2018.09.027.

[41] C.V. Loricera, M.C. Alvarez-Galvan, R. Guil-Lopez, A.A. Ismail, S.A. Al-Sayari, J.L. G. Fierro, Structure and Reactivity of sol–gel V/SiO_2 Catalysts for the Direct Conversion of Methane to Formaldehyde, Top. Catal. 60 (2017) 1129–1139.

[42] F. Arena, N. Giordano, A. Parmaliana, Working mechanism of oxide catalysts in the partial oxidation of methane to formaldehyde. ii. redox properties and reactivity of SiO_2, MoO_3/SiO_2, V_2O_5/SiO_2, TiO_2, and V_2O_5/TiO_2 systems, J. Catal. 167 (1997) 66–76.

[43] Š. Csáki, F. Lukáč, J. Veverka, T. Chráska, Preparation of Ti_3SiC_2 MAX phase from Ti, TiC, and SiC by SPS, Ceram. Int. 48 (2022) 28391–28395.

[44] M.A. El Saeed, F.A. Deorsola, R.M. Rashad, Optimization of the Ti_3SiC_2 MAX phase synthesis, Int. J. Refract. Met. Hard Mater. 35 (2012) 127–131, https://doi.org/10.1016/j.ijrmhm.2012.05.001.

[45] J.M. Córdoba, M.J. Sayagués, M.D. Alcalá, F.J. Gotor, Synthesis of Ti_3SiC_2 powders: reaction mechanism, J. Am. Ceram. Soc. 90 (2007) 825–830, https://doi.org/10.1111/j.1551-2916.2007.01501.x.

[46] M.W. Barsoum, T. El-Raghy, L.U.J.T. Ogbuji, Oxidation of Ti_3SiC_2 in air, J. Electrochem. Soc. 144 (1997) 2508.

[47] J. Ward, D. Bowden, E. Prestat, S. Holdsworth, D. Stewart, M.W. Barsoum, M. Preuss, P. Frankel, Corrosion performance of Ti_3SiC_2, Ti_3AlC_2, Ti_2AlC and Cr2AlC MAX phases in simulated primary water conditions, Corros. Sci. 139 (2018) 444–453.

[48] V. Figueiredo, E. Elangovan, G. Gonçalves, P. Barquinha, L. Pereira, N. Franco, E. Alves, R. Martins, E. Fortunato, Effect of post-annealing on the properties of copper oxide thin films obtained from the oxidation of evaporated metallic copper, Appl. Surf. Sci. 254 (2008) 3949–3954, https://doi.org/10.1016/j.apsusc.2007.12.019.

[49] L. De Los Santos Valladares, D.H. Salinas, A.B. Dominguez, D.A. Najarro, S. I. Khondaker, T. Mitrelias, C.H.W. Barnes, J.A. Aguiar, Y. Majima, Crystallization and electrical resistivity of Cu_2O and CuO obtained by thermal oxidation of Cu thin films on SiO_2/Si substrates, Thin Solid Films 520 (2012) 6368–6374, https://doi.org/10.1016/j.tsf.2012.06.043.

[50] H.S. Kim, J.W. Lim, S.J. Yun, M.A. Park, S.Y. Park, S.E. Lee, H.C. Lee, Fabrication and characterization of rapidly oxidized p-type Cu_2O films from Cu films and their application to heterojunction thin-film solar cells, Jpn. J. Appl. Phys. 52 (2013) 10MB17.

[51] C. Guillén, J. Herrero, Single-phase Cu_2O and CuO thin films obtained by low-temperature oxidation processes, J. Alloy. Compd. 737 (2018) 718–724, https://doi.org/10.1016/j.jallcom.2017.12.174.

[52] V.R. Palkar, P. Ayyub, S. Chattopadhyay, M. Multani, Size-induced structural transitions in the Cu-O and Ce-O systems, Phys. Rev. B 53 (1996) 2167–2170, https://doi.org/10.1103/PhysRevB.53.2167.

[53] M. Amer, M.W. Barsoum, T. El-Raghy, I. Weiss, S. Leclair, D. Liptak, The Raman spectrum of Ti_3 SiC_2, J. Appl. Phys. 84 (1998) 5817–5819.

[54] M.Y. Bashouti, K. Sardashti, J. Ristein, S.H. Christiansen, Early stages of oxide growth in H-terminated silicon nanowires: determination of kinetic behavior and activation energy, Phys. Chem. Chem. Phys. 14 (2012) 11877–11881, https://doi.org/10.1039/C2CP41709J.

[55] I. Persson, L.-Å. Näslund, J. Halim, M.W. Barsoum, V. Darakchieva, J. Palisaitis, J. Rosen, P.O.Å. Persson, On the organization and thermal behavior of functional groups on Ti_3C_2 MXene surfaces in vacuum, 2D Mater. 5 (2017) 15002.

[56] L.-Å. Näslund, I. Persson, XPS spectra curve fittings of $Ti_3C_2T_x$ based on first principles thinking, Appl. Surf. Sci. 593 (2022) 153442, https://doi.org/10.1016/j.apsusc.2022.153442.

[57] G.M. Bancroft, H.W. Nesbitt, R. Ho, D.M. Shaw, J.S. Tse, M.C. Biesinger, Toward a comprehensive understanding of solid-state core-level XPS linewidths: experimental and theoretical studies on the Si 2 p and O 1 s linewidths in silicates, Phys. Rev. B 80 (2009) 75405.

[58] F. Ureña-Begara, A. Crunteanu, J.-P. Raskin, Raman and XPS characterization of vanadium oxide thin films with temperature, Appl. Surf. Sci. (n.d.) 717–727. https://doi.org/DOI:101016/japsusc201701160.

[59] Y. Wang, Y. Lü, W. Zhan, Z. Xie, Q. Kuang, L. Zheng, Synthesis of porous Cu_2O/CuO cages using Cu-based metal–organic frameworks as templates and their gas-sensing properties, J. Mater. Chem. A 3 (2015) 12796–12803, https://doi.org/10.1039/C5TA01108F.

[60] C.-H. Chen, K. Koga, X-ray effects on the oxidation of Cu nanoparticles, Mater. Lett. 65 (2011) 1822–1824, https://doi.org/10.1016/j.matlet.2011.03.048.

[61] N. Pauly, S. Tougaard, F. Yubero, Determination of the Cu 2p primary excitation spectra for Cu, Cu2O and CuO, Surf. Sci. 620 (2014) 17–22, https://doi.org/10.1016/j.susc.2013.10.009.

[62] C. Racault, F. Langlais, R. Naslain, Solid-state synthesis and characterization of the ternary phase Ti3SiC2, J. Mater. Sci. 29 (1994) 3384–3392, https://doi.org/10.1007/BF00352037.

[63] X.H. Wang, Y.C. Zhou, Oxidation behavior of Ti_3AlC_2 powders in flowing air, J. Mater. Chem. 12 (2002) 2781–2785, https://doi.org/10.1039/B203644D.

[64] M.M. Koranne, J.G. Goodwin, G. Marcelin, Partial oxidation of methane over silica- and alumina-supported vanadia catalysts, J. Catal. 148 (1994) 388–391, https://doi.org/10.1006/jcat.1994.1219.

[65] J.M. Kanervo, M.E. Harlin, A.O.I. Krause, M.A. Bañares, Characterisation of alumina-supported vanadium oxide catalysts by kinetic analysis of H2-TPR data, Catal. Today 78 (2003) 171–180, https://doi.org/10.1016/S0920-5861(02)00326-7.

[66] O. Tursunov, L. Kustov, Z. Tilyabaev, Methanol synthesis from the catalytic hydrogenation of CO_2 over CuO–ZnO supported on aluminum and silicon oxides, J. Taiwan Inst. Chem. Eng. 78 (2017) 416–422, https://doi.org/10.1016/j.jtice.2017.06.049.

[67] Y.A. May, S. Wei, W.-Z. Yu, W.-W. Wang, C.-J. Jia, Highly efficient CuO/α-MnO2 catalyst for low-temperature CO oxidation, Langmuir 36 (2020) 11196–11206, https://doi.org/10.1021/acs.langmuir.0c00692.

[68] N. Agarwal, S.J. Freakley, R.U. McVicker, S.M. Althahban, N. Dimitratos, Q. He, D. J. Morgan, R.L. Jenkins, D.J. Willock, S.H. Taylor, C.J. Kiely, G.J. Hutchings, Aqueous Au-Pd colloids catalyze selective CH_4 oxidation to CH_3OH with O_2 under mild conditions, Science 358 (80) (2017) 223–227, https://doi.org/10.1126/science.aan6515.

[69] J.C. Mackie, Partial oxidation of methane: The role of the gas phase reactions, Catal. Rev. 33 (1991) 169–240.

[70] Q. Sun, J.-M. Jehng, H. Hu, R.G. Herman, I.E. Wachs, K. Klier, In situ Raman SPectroscopy during the Partial Oxidation of Methane to Formaldehyde over Supported Vanadium Oxide Catalysts, J. Catal. 165 (1997) 91–101.

[71] K. Otsuka, M. Hatano, , The catalysts for the synthesis of formaldehyde by partial oxidation of methane, J. Catal. 108 (1987) 252–255, https://doi.org/10.1016/0021-9517(87)90172-2.

[72] V. Amir-Ebrahimi, J.J. Rooney, Selective air oxidation of methane to formaldehyde using silica-supported MoCl5/R4Sn olefin metathesis catalysts, J. Mol. Catal. 50 (1989) L17–L22.

[73] A. Parmaliana, F. Frusteri, A. Mezzapica, M.S. Scurrell, N. Giordano, Novel high activity catalyst for partial oxidation of methane to formaldehyde, J. Chem. Soc. Chem. Commun. (1993) 751–753, https://doi.org/10.1039/C39930000751.

[74] V. Fornés, C. López, H.H. López, A. Martınez, Catalytic performance of mesoporous VOx/SBA-15 catalysts for the partial oxidation of methane to formaldehyde, Appl. Catal. A Gen. 249 (2003) 345–354.

[75] H. Berndt, A. Martin, A. Brückner, E. Schreier, D. Müller, H. Kosslick, G.-U. Wolf, B. Lücke, Structure and catalytic properties of VOx/MCM materials for the partial oxidation of methane to formaldehyde, J. Catal. 191 (2000) 384–400.

[76] Y. Li, D. An, Q. Zhang, Y. Wang, Copper-catalyzed selective oxidation of methane by oxygen: studies on catalytic behavior and functioning mechanism of CuO_x/SBA-15, J. Phys. Chem. C 112 (2008) 13700–13708.

[77] D. An, Q. Zhang, Y. Wang, Copper grafted on SBA-15 as efficient catalyst for the selective oxidation of methane by oxygen, Catal. Today 157 (2010) 143–148.

[78] R. Polnišer, M. Štolcová, M. Hronec, M. Mikula, Structure and reactivity of copper iron pyrophosphate catalysts for selective oxidation of methane to formaldehyde and methanol, Appl. Catal. A Gen. 400 (2011) 122–130, https://doi.org/10.1016/j.apcata.2011.04.022.

[79] Z. Sojka, R.G. Herman, K. Klier, Selective oxidation of methane to formaldehyde over doubly copper–iron doped zinc oxide catalysts via a selectivity shift

mechanism, J. Chem. Soc. Chem. Commun. (1991) 185–186, https://doi.org/10.1039/C39910000185.
[80] T. Akiyama, R. Sei, S. Takenaka, Partial oxidation of methane to formaldehyde over copper–molybdenum complex oxide catalysts, Catal. Sci. Technol. 11 (2021) 5273–5281, https://doi.org/10.1039/D1CY00511A.
[81] N.D. Spencer, C.J. Pereira, V_2O_5· SiO_2-catalyzed methane partial oxidation with molecular oxygen, J. Catal. 116 (1989) 399–406.
[82] J. Zhang, V. Burklé-Vitzthum, P.M. Marquaire, G. Wild, J.M. Commenge, Direct conversion of methane in formaldehyde at very short residence time, Chem. Eng. Sci. 66 (2011) 6331–6340.
[83] S. Mansouri, O. Benlounes, C. Rabia, R. Thouvenot, M.M. Bettahar, S. Hocine, Partial oxidation of methane over modified Keggin-type polyoxotungstates, J. Mol. Catal. A Chem. 379 (2013) 255–262.
[84] K. Yang, J. Li, Z. Zhao, Z. Liu, Observation of induction period and oxygenated intermediates in methane oxidation over Pt catalyst, IScience (2023).
[85] B. Frank, J. Zhang, R. Blume, R. Schlögl, D.S. Su, Heteroatoms increase the selectivity in oxidative dehydrogenation reactions on nanocarbons, Angew. Chem. Int. Ed. 48 (2009) 6913–6917.
[86] K. Chen, A. Khodakov, J. Yang, A.T. Bell, E. Iglesia, Isotopic tracer and kinetic studies of oxidative dehydrogenation pathways on vanadium oxide catalysts, J. Catal. 186 (1999) 325–333, https://doi.org/10.1006/jcat.1999.2510.